Self-Assembled Thermally Highly Stable 1-Dimensional Proton Arrays

ARTICLE *in* THE JOURNAL OF PHYSICAL CHEMISTRY B · JUNE 2010

Impact Factor: 3.3 · DOI: 10.1021/jp101990f · Source: PubMed

Self-Assembled Thermally Highly Stable 1-Dimensional Proton Arrays

In-Chul Hwang, Sung Woo Heo, N. Jiten Singh, Jung Woo Lee, Young Chun, Seung Bin Baek, Kyeong Sik Jin, Moonhor Ree, Hee Cheon Lee,* Seung Bin Kim,* and Kwang S. Kim*

Department of Chemistry, Center for Superfunctional Materials, Center for Basic Sciences, Pohang University of Science and Technology, Pohang 790-784, Korea

Received: March 5, 2010; Revised Manuscript Received: April 25, 2010

From a red proton complex of aldehyde derivatives of polyaromatic hydrocarbon with strong intermolecular hydrogen bonding, which are novel examples of intermolecular proton-bonded aldehydes of polyaromatic hydrocarbons, we find one-dimensional proton arrangement. The complex formed as 9-antraldehyde (Ant-CHO) reacts with $HAuCl_4$ to form $[(Ant\text{-}CHO)_2H]^+[AuCl_4]^-$ under dry condition, which are confirmed by single-crystal structure determination and infrared spectra analysis at varying temperatures. Since the compounds of distinctively hydrophobic nature are soluble only in limited organic polar solvents, the strong hydrogen bonds are clearly observed from both the electron density of X-ray analysis and the characteristic signature of the IR frequency. The proton complex units have the typical $O-H^+-O$ distance of the strong hydrogen bond similar to the Zundel-like cationic hydrogen bond (where two O atoms share a proton in the midpoint of the short O−O distance of ∼2.4 Å). The chemical shift of 20.18 ppm originated from the protons of the $O-H^+-O$ hydrogen bonds would be the largest downfield shifted value among those of protons in O−H···O bonds reported in various solid materials, indicating very short strong hydrogen bonds for the $O-H^+-O$. The complexes are stabilized with the $\pi-\pi$ intermolecular interactions of the polyaromatic hydrocarbon ligands, resulting in layered structures. The spectral signatures around ∼900, ∼1200, and ∼1700 cm^{-1} for the Zundel-like proton bond are clearly characterized.

I. Introduction

The molecular self-assembly constructs diverse supramolecular structures with noncovalent intermolecular interactions.[1] While diverse π-interactions[2] are very useful for stabilizing various intriguing structures such as nanomaterials[3] and biomolecules,[4] diverse H-bonding types[5] play important roles in constructing interesting H-bonded structures.[6] These H-bonds are classified as weak to strong H-bonds in terms of strength.[7] The neutral −O−H···O− type, typical of hydrogen bonding, is ubiquitous, as can be seen in water. The anionic H-bond type of $-(O\cdots H\cdots O)^-$− is associated with oxyanions and plays a vital role in lowering the transition barrier in the catalytic mechanism of various biologically important enzymes.[8] These short strong H-bonds (SSHB) are often considered as low-barrier H-bonds (LBHB). On the other hand, strong cationic intra/intermolecular hydrogen bonds are present in malonate[9] and protonated water clusters.[10] Some cationic H-bonded or proton-bonded complexes with organic ligands in crystals,[11,12] in solution,[11] and in the gas phase[13] have been reported. In this cationic H-bond, the charge of H is between the charge of a proton and the charge of a neutral H atom. Thus, this $-(O-H-O)^+-$ or $-O-H^+-O-$ bond is often called a proton bond.[13] Here, we report novel proton arrays in the proton-bonded crystal structure of $[(Ant\text{-}CHO)_2H]^+[AuCl_4]$ (**I**), which is stabilized particularly by $\pi-\pi$ interactions. The thermal property of the proton bonded complex **I** is investigated by using infrared (IR) spectra, X-ray diffraction, and differential scanning calorimetry (DSC) analysis. The temperature dependent IR spectra are employed to characterize important vibrational modes associated with $O-H^+-O$ and to investigate the temperature dependent distance changes of the H-bond distances and π-stacking distances together with the X-ray analysis, solid-state NMR spectroscopy (^{1}H magic-angle spinning (MAS) NMR experiments), and density functional theory (DFT) calculations.

* To whom correspondence should be addressed. E-mail: kim@postech.ac.kr (K.S.K.); sbkim@postech.ac.kr (S.B.K.); hcl@postech.ac.kr (H.C.L.). Tel: (+82)-54-279-2110, Fax: (+82)-54-279-8137.

II. Experimental Section

II.1. Synthesis and Analysis of $[(Ant\text{-}CHO)_2H]^+[AuCl_4]^-$ (I). Compound **I** (Figure 1) was prepared by the reaction between Ant-CHO (150 mg, 0.728 mmol) with $HAuCl_4\cdot 3(H_2O)$ (145 mg, 0.368 mmol) in CH_3CN/CH_3Cl (or CH_3CN/CH_2Cl_2) solution at 20 °C. The red plate crystals were obtained in the inert gas system (Argon or N_2) by the slow evaporation of solvents at room temperature for 3 days. After isolation it was characterized with the X-ray single crystal structure analysis, the IR spectroscopy, and ^{1}H-MAS NMR spectroscopy. MALDI-TOF mass spectrometric analysis: $m/z = 207$ $[(C_{15}H_{10}O) + H^+]$, 339 $[AuCl_4^-]$.

II.2. FT-IR Spectral Analysis. The Fourier Transform infrared (FT-IR) spectra were measured at a spectral resolution of 4 cm^{-1} with a Bruker IFS 66v/S FTIR spectrometer equipped with a liquid nitrogen-cooled mercury cadmium telluride (MCT) detector and an AABSPEC 2000 multimode experimental chamber. The sample was studied as a powder dispersed in a KBr pellet. Variable temperature spectra were measured with an AABSPEC 2000 multimode experimental chamber. All FTIR spectra were measured by coadding 256 scans. The sample and source compartments were evacuated to 1 mbar. FT-IR spectra in the KBr window (500 to 4000 cm^{-1} range) of the red plate crystal of **I** is recorded every 10 K in the temperature range from 123 to 423 K.

II.3. Differential Scanning Calorimetry Analysis. DSC thermograms were measured under a nitrogen atmosphere over

10.1021/jp101990f
Published on Web 05/06/2010

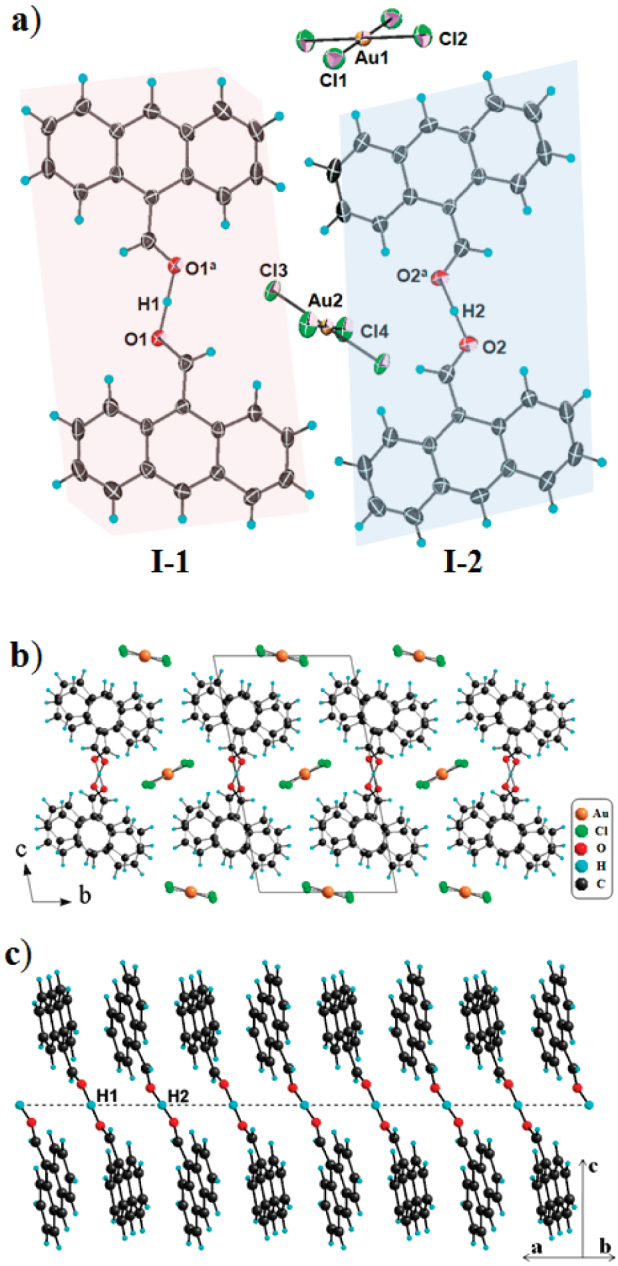

Figure 1. Structure of **I** showing the proton arrays: (a) single crystal structure (thermal ellipsoids set at 50% probability), indicating two types of proton complexes $[(\text{Ant-CHO})_2\text{H}]^+$ (**I**-1 and **I**-2); (b) projection of the unit cell structure **I** along the *a*-axis; (c) proton array of the lined-up protons [d(H1···H2) = 3.793(3) Å] along with the $\pi-\pi$ intermolecular interactions [d(C···C) ≈ 3.38(3) Å] at 243 K. The proton lies on the inversion center.

the temperature range 173−673 K using a calorimeter (model DSC-220CU, Seiko instruments) calibrated with indium and tin standards. The heating and cooling rates were 10.0 K min^{-1}.

II.4. Solid-State NMR spectroscopy. ^{1}H magic-angle spinning (MAS) NMR experiments were performed on a Varian Unity Inova 600 spectrometer with a 14.1 T wide bore magnet (Oxford Instruments, Cambridge, U.K.) corresponding to the proton frequency of 600 MHz. The crystalline powder sample of complex **I** was packed in zirconia rotor (o.d. 2.5 mm). The spinning speed was kept at 25 kHz ± 5 Hz during the experiments and the depth-pulse was applied to obtain the ^{1}H resonances with the background signals from the probe head suppressed. ^{1}H MAS NMR data were collected with 16 scans, 10 s relaxation delay, 4 K data points, and a spectral width of 200 kHz. All ^{1}H chemical shift values were referenced externally to tetramethylsilane (TMS).

II.5. X-ray Crystal Structure Analysis. The crystal of **I** was measured on Bruker-SMART-APEX-diffractometer (λ = 0.710 73 Å) at 243 K and ADSC Quantum 210 CCD diffractometer with synchrotron radiation (λ = 0.800 00 Å) at Macromolecular Crystallography Wiggler Beamline 4A, Pohang Accelerator Laboratory (PAL). Using the latter, the low-temperature diffraction data from both single crystals of **I** (0.10 × 0.05 × 0.05 mm^3) were collected from 100 to 333 K. The crystal was rotated through 360°. The raw data were processed and scaled using the program HKL2000. The structure was solved by direct methods, and the refinements were carried out with full-matrix least-squares on F^2 using the Bruker SHELXTL program package.[14] The data collection and refinement are summarized in Supporting Information: Tables S1, S2, and S3.[15]

Further details on the crystal structure investigations are available in the Supporting Information and may be obtained from the Cambridge Crystallographic Data Centre (via www.ccdc.cam.ac.uk) on quoting the depository numbers CCDC-660016 ($[\text{H}(\text{C}_{15}\text{H}_{10}\text{O})_2]^+[\text{AuCl}_4]^-$).

III. Results and Discussion

The interaction of 9-antraldehyde (Ant-CHO) with $HAuCl_4$ in mixed solution ($CH_3CN/CHCl_3$ or CH_3CN/CH_2Cl_2) leads to the proton complex **I**. Slow evaporation of organic solvents crystallizes proton complexes with other diverse organic ligands (urea, acetamide, acetanilide, benzoyl, formamide, etc.) as a colorless or yellow color in the solid state.[16] The single crystal of **I** is red due to the existence of proton bonds in the solid state, which will be discussed later.

The crystal structure **I** (Figure 1) shows the intermolecular $\pi-\pi$ interactions[17] of polyaromatic hydrocarbon (PAH) compounds as well as the proton-bonded aldehyde dimers. It is a novel example for a linear proton bonded polyaromatic hydrocarbon complexes. Neither the crystal structure of proton bonded aldehydes nor that of proton bonded PAH compounds is reported in the literature. The unit cell structure contains two crystallographically independent proton complexes $[(\text{Ant-CHO})_2\text{H}]^+$ (**I**-1 and **I**-2) and two anions $[AuCl_4]^-$ that are arranged between two chains of proton bonding planes.[15]

Most molecular packing systems of PAH derivates are the herringbone type[18] with the intermolecular interactions comprising $\pi-\pi$ and H$-\pi$ interactions. For example, the anthracene and pyrene molecules have been found to have two structural forms: (i) the sandwich-herringbone structure with a H$-\pi$ interaction between the dimers, each of which is composed of two parallel stacks at the normal pressure, and (ii) the high-pressure polymorph with the graphite-like $\pi-\pi$ stacking (vertical distance 3.5 Å and the off-center ring displacement 1.61 Å) at high pressure (0.3−0.5 GPa).[19]

However, the crystal lattice structure (**I**) is composed of almost nondisplaced but slightly twisted $\pi-\pi$ stacking interactions between two anthracene moieties (**I**-1 and **I**-2) in alternating layers. The average perpendicular lengths of the intermolecular $\pi-\pi$ stacking between anthracenyl moieties are 3.386(2) and 3.356(2) Å, respectively. The crystal structure also provides 1.70° (for α), 17.67° (for β), and 51.46° (for γ) for the twist angles. (See the definition of angles (α, β, γ) in the Supporting Information: Figures S2 and S3.)[15] The layer-to-layer distance of anthracenyl aromatic rings is significantly shorter than that of graphite (~3.4 Å). The square planar structure of counteranions $[AuCl_4]^-$ is stabilized with linear intermolecular H-bonds (C(=O)−H···Cl; d(H···Cl) = 2.738 Å). They are lined up

along the *a*-axis and constructed on an ionic salt layer along the *b*-axis (Figure 1b).

Figure 1c shows the intriguing one-dimensional proton (quasi-)arrays where the lined-up interproton distance *d*(H1···H2) is 3.793 Å along the *a*-axis. A proton-like H atom is coordinated linearly with two oxygen atoms of the π-electron rich polyaromatic hydrocarbon ligands. Series of these protons form one-dimensional proton arrays, which are stabilized by the dipole−dipole interactions between neighboring O−H−O groups and by the $\pi-\pi$ stacking interactions between polyaromatic rings. These proton arrays are particularly interesting because this kind of self-assembly could be utilized to line up charged atoms or moieties. The proton arrays are characterized from the X-ray structure as central hydrogen atoms (H1 and H2) lying on the inversion center in between two oxygen atoms of Ant-CHO. The cationic H-bond distances are 2.440(4) Å (O1···O1^a ($2-x, 2-y, 1-z$)) and 2.412(4) Å (O2···O2^a ($2-x, 2-y, 1-z$)) (Figure 1a), which are between the O···O distances of $H_5O_2^+$ (2.395(4) Å at 225 K) and protonated benzophenone (2.470(3) Å at 198 K) in the solid state.[20] The crystallographic electron densities of the bridged hydrogen atoms (H1 and H2) are weakly distributed between O1 and O1^a (also O2 and O2^a) (Figures S4 and S5, Supporting Information).[15] Each central O−H$^+$−O unit is linear (180°), and the O−H bond distances are 1.220(4) and 1.206(4) Å. Owing to the proton bonding, the C═O bond length increases to 1.248(6) and 1.255(7) Å, as compared with the value of 1.21 Å in the crystalline 9-antraldehyde.[18]

The natural bond orbital charge of the H$^+$ atom in **I** is calculated to be +0.5 au, which is between the charge of a pure proton (+1.0 au) and the charge of hydrogen atom (0.0 au) at the DFT level (BLYP/6-31G*). As compared with neutral and anionic hydrogen bonds, positively charged hydrogen bonds have a more positively charged value for the H atom between two oxygen atoms, showing more of the proton-bond characteristics. Nevertheless, there is net excess electron density of half an elementary charge around the proton, which allows us to obtain the electron density in the X-ray analysis.

In the cationic H-bonds or proton bonds, the interoxygen distance [*d*(O···O)] of the cationic (−O−H−O−)$^+$ moiety as well as $H_5O_2^+$ is 2.4−2.5 Å, which is slightly shorter than that of anionic H-bonds.[21] This is highly contrasted with other H-bonds. In anionic H-bond systems, the interoxygen distance of the anionic (−O−H−O−)$^-$ moiety as well as $H_3O_2^-$ is generally 2.5−2.6 Å. Here, the repulsion between the two O atoms in the anionic moiety is stronger than that in the cationic moiety, resulting in a slightly longer H-bond length in the anionic moiety. In the case of neutral H-bonds, interoxygen distance is 2.7−2.9 Å.[22] For H-bond relay systems (composed of consecutive H-bonds), the interoxygen distances become shorter and stronger (down to ~2.64 Å).[23]

As the temperature increases from 100 to 300 K, the unit cell volume increases and the two different O−H$^+$−O distances [*d*(O1···O1^a) and *d*(O2···O2^a)] increase by 0.025 and 0.027 Å (Figures 2a and S4, Supporting Information). The vertical π-stacking distance increases by 0.056 Å (Figure S3, Supporting Information).[15] The temperature-dependent distance changes are clear with much larger varation than the error ranges. As the temperature increases, the increase in the O−H$^+$−O distance is naturally expected due to the slightly weakened proton bond strength. This increase would not be affected significantly by the change in the $\pi-\pi$ stacking distance because the $\pi-\pi$ interaction is weak. Since most H-bonding weakens as the temperature increases, it is expected that the breaking of the

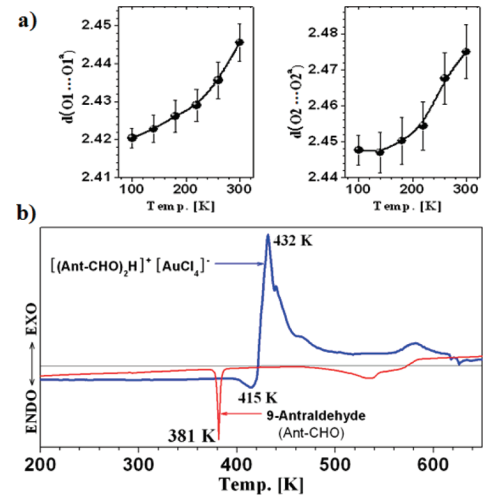

Figure 2. (a) Temperature dependence of the *d*(O1···O1^a)/*d*(O2···O2^a) distances from the synchrotron X-ray crystal structure analysis of **I** (100−300 K; distances in Å). (b) DSC analysis of **I** (blue) compared with that of 9-antraaldehyde (red). The temperature was increased by 10 K/min in the range 190−700 K.

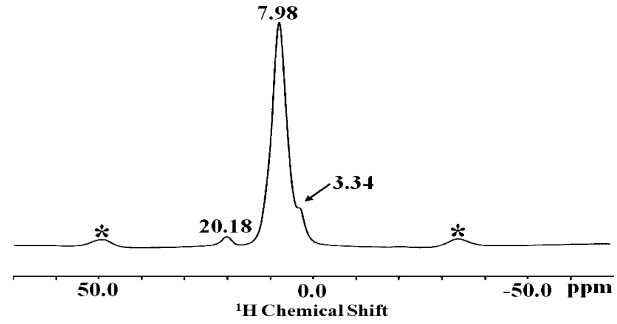

Figure 3. Normal 600 MHz ^{1}H MAS NMR spectrum (25 kHz) of proton complex **I**. Asterisks indicate spinning side bands. Spectra were collected with 16 scans, 10 s relaxation delays, 4 K data points, and a spectral width of 200 kHz. The chemical shifts are based on reference to the standard tetramethylsilane.

present H-bonds is also expected somewhere around the water boiling point, which will result in phase transition.

Thus, the thermal structural transformations have been studied with differential scanning calorimetry (DSC) in the temperature range 190−700 K (Figure 2b). There are no significant phase changes below 400 K. The proton-bonded complex undergoes a gradual endothermic to exothermic transition at 415 K as it decomposes. Its thermal stability is considerably enhanced as compared to that of Ant-CHO (381 K) and the water boiling point (373 K), which indicates that the proton bond is much stronger than the normal H-bond. Over the decomposion temperature (423 K), the red compound changes to black with the formation of black charred material.

The ^{1}H MAS NMR spectra of proton complex **I** show two well-separated ^{1}H resonances (Figure 3). The broad chemical shift around 7.98 ppm arises from the H atoms of Ant-CHOs, while the smaller high-frequency resonance around 20.18 ppm originates from the protons of the O−H$^+$−O hydrogen bonds. It is noted that this chemical shift is much more downfield shifted as compared to those of protons in O−H···O bonds reported in various solid materials, which generally ranges 2−10 ppm (and can be down to ~18 ppm for very high SSHBs).[24] The resonance of a small peak (3.34 ppm) originates from the protons directly placed above and/or below different planar anthracene moieties. The environment of such protons could

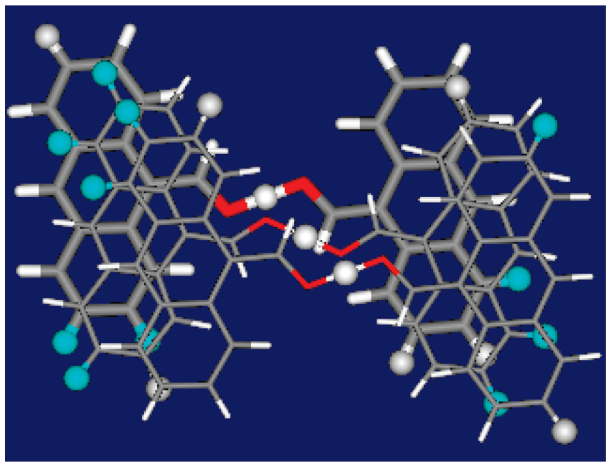

Figure 4. On the crystal geometry, the BLYP/6-31G* optimized geometries of $(Ant\text{-}CHO)_2H^+$ overlapped, forming the trimer structure to simulate the overall crystal packing effect. Dihedral angles of the optimized geometry are slightly modified to closely fit the crystal geometry. After deleting the crystal coordinate, we have obtained the trimer structure shown above. We have calculated the NMR properties of the monomer, dimer, and trimer forms using the GIAO method at the BLYP/6-31G* level of theory.

TABLE 1: Calculated Chemical Shifts (ppm) of the Monomer, Dimer, and Trimer Forms of $(Ant\text{-}CHO)_2H^+$

	HH^+ (ppm)	aromatic and aldehydic hydrogen (ppm)
monomer	24.70	5.2−11.4 (7.9): 20 H's
dimer	24.04, 24.15	4.0−11.3 (7.4): 40 H's
trimer	23.76, **20.25**, 24.52	1.9−4.7 (**4.1**): 18 H's [cyan color: 1.9−4.5 (3.8): 11 H's] [gray color: 4.5−4.7: 7 H's] 4.9−13.2 (**7.3**): 42 H's

be more shielded by the opposing field generated by π-electrons (ring current effect).

In the trimer structure of $(Ant\text{-}CHO)_2H^+$ which simulates the crystal packing effect, the chemical shift of the proton in the $O-H^+-O$ bond is 20.25 ppm, which is smaller than those of the monomer and dimer forms (~24 ppm). For the aromatic hydrogen atoms that lie on and below the anthracene ring, the chemical shifts are upfield shifted to an average value of 3.8 ppm (protons shown as cyan color in Figure 4), which is in close agreement with the experimental value of 3.34 ppm. Meanwhile, the chemical shift of the rest of the aromatic and aldehydic protons is predicted to have an average value of 7.3 ppm. These individual chemical shifts of the ^1H MAS NMR spectrum calculated with DFT (Figure 4, Table 1) show that the crystal packing also plays a role in determining chemical shifts of the protons in $O-H^+-O$ bonds and the aromatic and aldehydic protons.

The spectral features of various organic proton bonds have been studied in the gas phase.[13] In the spectral studies of the proton bonded crystal systems, the proton-bonded peaks could be conjectured to be very broad (600−1500 cm^{-1}). However, according to the DFT analysis, this broad band is not the OH^+O features but the feature of many complex modes generated upon the dimer formation through the proton bond (see Supporting Information).[15] The IR spectra of **I** below the decomposition temperature show an interesting change in the peak pattern as compared with those of Ant-CHO (Figure 5). The vibration modes ν(C═O) and ν(C−H) marked with an asterisk (1668 and 2770/2855 cm^{-1}) for the aldehyde groups of Ant-CHO disappear due to the formation of proton complexes. As for the new

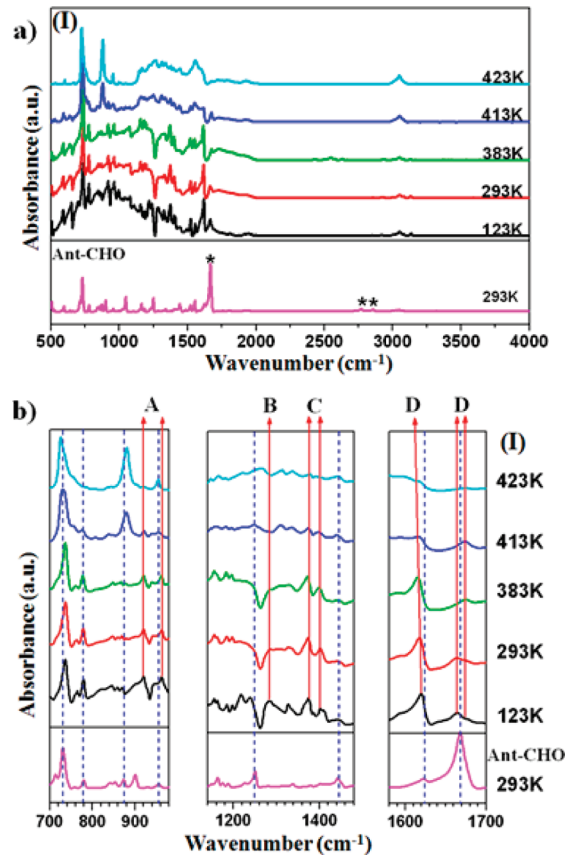

Figure 5. IR spectra of **I** at selected temperatures (123−423 K). (a) Spectra in the range 500−4000 cm^{-1} for **I** and Ant-CHO. (b) Zoom-in frequency ranges of the (O−H−O) mode. At 293 K, the characteristic frequencies/cm^{-1} of Ant-CHO are at 901 [ω(Ant)], 1250 [δ_i(CH) of Ant], and 1668 [ν(C═O) of CHO]. At temperatures between 123 and 413 K, the characteristic frequencies/cm^{-1} of **I** appear at 921 and 962 (**A**) [ν(O−H^+−O)], at 1281 (**B**) [δ_o(OHO)], at 1373 and 1401 (**C**) [δ_i(C−H) of CHO], and at ~1620 and ~1664 (**D**) [δ_i(OH^+O)]. Above 413−423 K, these frequencies disappear, indicating the breaking of the O−H^+−O proton bonds [ν, stretching; δ_i, in-plane bending; δ_o, out-of-plane bending; ω, wagging]. Around 403−413 K, these peaks disappear and the Ant-CHO peaks reappear, indicating the breaking of the proton-bonded dimer into monomers.

absorption vibration modes of the O−H^+−O moiety in the FTIR spectra of both proton complexes, we assign the stretching and bending modes as ν_{as}(919, 961 cm^{-1}) and δ(1620 cm^{-1}) at 123 K. This assignment was made from the investigation of the spectral changes upon raising the temperature from 123 to 423 K as well as from the DFT(B3LYP/6-31G*) predicted IR spectra (Tables 1 and S4, Supporting Information).[15] Above 383 K, the ν(C═O) band does not appear at 1668 cm^{-1}, and the δ_i(OHO) bands start losing their identity. Thus, **I** does not return to the pure Ant-CHO even after the OH^+O bond breaks but transforms to other compounds that we could not characterize. At 413 and 423 K, the broad vibration band range (500−900 cm^{-1}) disappears. The temperature dependent IR spectral analysis suggests that the OH^+O moiety is stable up to 383 K. The OH^+O bond starts to break at 413 K and is completely dissociated at 423 K. Thus, we again note that the OH^+O bonding is highly stabilized up to ~400 K, much higher than the water boiling point 373 K.

DFT calculations of Ant-CHO and its protonated form (Ant-CHO-H^+) show that the charge transfer from the aromatic ring to the O−H^+ moiety is small (Figures S6 and S7, Supporting Information).[15] As Ant-CHO changes to Ant-CHO^+, the bond distance between the aromatic carbon and aldehydic carbon

TABLE 2: Selected Experimental IR-Absorption Peaks (Frequencies in cm^{-1}) for the Proton Complex I (at 123−423 K) along with the Predicted Frequencies at the BLYP/6-31G* Level of Theory[a,b]

$[(Ant\text{-}CHO)_2H]^+ [AuCl_4]^-$ (**I**)						
expt						
123 K	293 K	383 K	413 K	423 K	calc	mode
921	919	919	919	nv	883 s	ν(O−H) of OHO
962	962	961	961	nv	938 s	
1281	1283	1284	nv	nv	1295	δ_o(OHO)
1620	1617	1615	1618	nv	1577	δ_i(OHO) + δ_i(C−H) of CHO
1664	1663	u	u	nv	1631 s	
u	u	1673	1673	1674		

[a] ν: stretching. δ_i: in plane bending. δ_o: out of plane bending. [b] BLYP/6-31G* frequencies (f^i) are scaled (f^s) exponentially with $\alpha = 0.9296 \times 10^{-5}$ $\{f^s = f^i \exp[-\alpha f^i]\}$.[25] (nv, not visible; u, unable to assign; s, strong).

decreases from 1.48 to 1.40 Å, which is comparable to 1.47 and 1.41 Å in the crystal structures of Ant-CHO and **I,** respectively.

The protonation of Ant-CHO leads to the extended delocalization of the π-electrons, resulting in lowering the band gap, namely, decreasing the $\pi-\pi^*$ electron transfer energy in Ant-CHO-H^+. This results in a color change from yellow to red. The red crystal contains the short strong hydrogen bonding, so that the proton complex is very stable without a color change under dry conditions at room temperature for a long period. This compound is thermally stable only in the solid state under dry conditions. It is moisture sensitive and easily dissociated in polar organic solvents (MeOH, EtOH, $CHCl_3$, CH_2Cl_2, CH_3CN, etc.). In various solvents (H_2O, alcohol, CH_3CN, etc.), **I** is segregated very sensitively into a yellowish orange solution ($HAuCl_4$) and a yellow suspension (Ant-CHO). With anhydrous sulfuric acid (98%) in CH_2Cl_2, the polyaromatic aldehyde ligands form protonated aldehyde groups. Upon dissolving **I** in these polar solvents, the crystalline red color disappears due to the breakage of the O−H^+−O bond.

IV. Conclusion

The intriguing one-dimensional proton arrays formed in polyaromatic hydrocarbon proton complex **I** are investigated by diffractometric and spectroscopic techniques. The charge of the hydrogen in the O−H^+−O bond is 0.5 au, suggesting that this H^+ shows the characteristics between a proton and a neutral H atom. The thermal structural transformations by the analysis of FTIR spectra and DSC show that the proton bonds break at 415 K (**I**). Owing to the $\pi-\pi$ interactions, the proton-bonded system is highly stabilized to ~400 K. The characteristic peaks of the O−H^+−O vibrational spectra of **I** at room temperature are 919 and 962 cm^{-1} for the stretching modes and 1617 and 1663 cm^{-1} for the bending modes. The extremely large proton chemical downshift of 20.18 ppm in the ^1H MAS NMR spectrum of the proton complex originates from the protons of the O−H^+−O hydrogen bonds. We find that the dipole−dipole interactions between neighboring O−H^+−O moieties together with the weak $\pi-\pi$ interactions make the linear proton (quasi-)-array in the crystal stable at much higher temperatures above the water boiling point. This assembling architecture could be utilized to construct novel self-assembling architecture of linear arrays of charged atoms and moieties.

Acknowledgment. This work was supported by KRF (2006-353-C00028), NRF (EPB Center: 2009-0063312, WCU: R32-2008-000-10180-0, GRL, BK21), and KISTI (KSC-2008-K08-0002). The temperature-dependent X-ray characterization was carried out using the synchrotron source at PAL (Beamline 6B).

Supporting Information Available: CIF file for **I**. Figures showing the unit cell structure of **I**, crystal data for **I**, bond lengths and angles for **I**, X-ray crystal data for **I**, symbols for structural analysis of distances and angles in **I**, temperature dependence of perpendicular π-stacking distances, temperature dependent distances, difference electron density plots, HOMO and LUMO molecular orbitals, and NBO charges. Table and text of additional details of IR spectra analysis. This material is available free of charge via the Internet at http://pubs.acs.org.

References and Notes

(1) (a) Meyer, E. A.; Castellano, R. K.; Diederich, F. *Angew. Chem., Int. Ed.* **2003**, *42*, 1210–1250. (b) Hoeben, F. J. M.; Jonkheijm, P.; Meijer, E. W.; Schenning, A. P. H. J. *Chem. Rev.* **2005**, *105*, 1491–1546. (c) Singh, N. J.; Lee, H. M.; Hwang, I.-C.; Kim, K. S. *Supramol. Chem.* **2007**, *19*, 321–332.

(2) (a) Hobza, P.; Selzle, H. L.; Schlag, E. W. *Chem. Rev.* **1994**, *94*, 1767–1784. (b) Tarakeshwar, P.; Choi, H. S.; Kim, K. S. *Chem. Rev.* **2000**, *100*, 4145–4185. (c) Kim, D.; Hu, S.; Tarakeshwar, P.; Kim, K. S.; Lisy, J. M. *J. Phys. Chem. A* **2003**, *107*, 1228–1238. (d) Singh, N. J.; Min, S. K.; Kim, D. Y.; Kim, K. S. *J. Chem. Theor. Comput.* **2009**, *5*, 515–529. (e) Guin, M.; Patwari, G. N.; Karthikeyan, S.; Kim, K. S. *Phys. Chem. Chem. Phys.* **2009**, *11*, 11207–11212.

(3) (a) Singh, N. J.; Lee, H. M.; Suh, S. B.; Kim, K. S. *Pure Appl. Chem.* **2007**, *79*, 1057–1075. (b) Lee, J. Y.; Hong, B. H.; Kim, W. Y.; Min, S. K.; Kim, Y.; Jouravlev, M. V.; Bose; Kim, K. S.; Hwang, I.-C.; Kaufman, L. J.; Wong, C. W.; Kim, P.; Kim, K. S. *Nature* **2009**, *460*, 498–501. (c) Nishizawa, T.; Tajima, K.; Hashimoto, K. *J. Mater. Chem.* **2007**, *17*, 2440–2445.

(4) (a) Burley, S. K.; Petsko, G. A. *Science* **1985**, *229*, 23–28. (b) Jureka, P.; Hobza, P. *J. Am. Chem. Soc.* **2003**, *125*, 15608–15613. (c) Cerny, J.; Kabelac, M.; Hobza, P. *J. Am. Chem. Soc.* **2008**, *130*, 16055–16059.

(5) (a) Grabowski, S. J. *Hydrogen Bonding-New Insights*; Springer: Dordrecht, The Netherlands, 2006. (b) Scheiner, S. *Hydrogen Bonding. A Theoretical Perspective*; Oxford University Press: New York, 1997. (c) Lee, H. M.; Kumar, A.; Kolaski, M.; Kim, D. Y.; Lee, E. C.; Min, S. K.; Park, M.; Choi, Y. C.; Kim, K. S. *Phys. Chem. Chem. Phys.* **2010**, DOI: 10.1039/B925551F.

(6) (a) Barbour, A. J.; Orr, G. W.; Atwood, J. L. *Nature* **1998**, *393*, 671–673. (b) Hong, B. H.; Lee, J. Y.; Lee, C.-W.; Kim, J. C.; Bae, S. C.; Kim, K. S. *J. Am. Chem. Soc.* **2001**, *123*, 10748–10749. (c) Hong, B. H.; Bae, S. C.; Lee, C.-W.; Jeong, S.; Kim, K. S. *Science* **2001**, *294*, 348–351. (d) Wang, D.; Lu, M.; Arora, P. S. *Angew. Chem., Int. Ed.* **2008**, *47*, 1879–1882. (e) Vasudev, P. G.; Chatterjee, S.; Ananda, K.; Shamala, N.; Balaram, P. *Angew. Chem., Int. Ed.* **2008**, *47*, 6430–6432.

(7) Pak, C.; Lee, H. M.; Kim, J. C.; Kim, D.; Kim, K. S. *Struct. Chem.* **2005**, *16*, 187–202.

(8) (a) Cleland, W. W.; Kreevoy, M. M. *Science* **1994**, *264*, 1887. (b) Kim, K. S.; Kim, D.; Lee, J. Y.; Tarakeshwar, P.; Oh, K. S. *Biochemistry* **2002**, *41*, 5300–5306. (c) Kim, K. S.; Oh, K. S.; Lee, J. Y. *Proc. Natl. Acad. Sci. U.S.A.* **2000**, *97*, 6373–6378.

(9) (a) Madsen, D.; Flensburg, C.; Larsen, S. *J. Phys. Chem. A* **1998**, *102*, 2177–2188. (b) Perrin, C. L.; Nielson, J. B. *Annu. Rev. Phys. Chem.* **1997**, *48*, 511–544.

(10) (a) Asmis, K. R.; Pivonka, N. L.; Santambrogio, G.; Brummer, M.; Kaposta, C.; Neumark, D. M.; Wöste, L. *Science* **2003**, *299*, 1375–1377. (b) Miyazaki, M.; Fujii, A.; Ebata, T.; Mikami, N. *Science* **2004**, *304*, 1134–1137. (c) Shin, J. -W.; Hammer, N. I.; Diken, E. G.; Johnson, M. A.; Walters, R. S.; Jaeger, T. D.; Duncan, M. A.; Christie, R. A.; Jordan,

K. D. *Science* **2004**, *304*, 1137–1140. (d) Headrick, J. M.; Diken, E. G.; Walters, R. S.; Hammer, N. I.; Christie, R. A.; Cui, J.; Myshakin, E. M.; Duncan, M. A.; Johnson, M. A.; Jordan, K. D. *Science* **2005**, *308*, 1765–1769. (e) Singh, N. J.; Park, M.; Min, S. K.; Suh, S. B.; Kim, K. S. *Angew. Chem., Int. Ed.* **2006**, *45*, 3795–3800. (f) McCunn, L. R.; Roscioli, J. R.; Johnson, M. A.; McCoy, A. B. *J. Phys. Chem. B* **2008**, *112*, 321–327. (g) Niedner-Schatteburg, G. *Angew. Chem., Int. Ed.* **2008**, *47*, 1008–1011.

(11) (a) Kleinman, E. F.; Bordner, J.; Newhouse, B. J.; MacFerrin, K. *J. Am. Chem. Soc.* **1992**, *114*, 4945–4946. (b) Hill, C. L.; Bouchard, D. A.; Kadkhodayan, M.; Williamson, M. M.; Schmidt, J. A.; Hilinski, E. F. *J. Am. Chem. Soc.* **1988**, *110*, 5471–5479. (c) Esterhuysen, M. W.; Raubenheimer, H. G. *Eur. J. Inorg. Chem.* **2003**, 3861–1869.

(12) (a) Gille, P.; Bertolasi, V.; Pretto, L.; Ferretti, V.; Gilli, G. *J. Am. Chem. Soc.* **2004**, *126*, 3845–3855. (b) Steiner, T.; Majerz, I.; Wilson, C. C. *Angew. Chem., Int. Ed.* **2001**, *40*, 2651–2654.

(13) Roscioli, J. R.; McCunn, L. R.; Johnson, M. A. *Science* **2007**, *316*, 249–254.

(14) (a) Sheldrick, G. *Program for Crystal Structure Solution*; Universität Göttingen: Göttingen, Germany, 1986. (b) Sheldrick, G. *Program for Crystal Structure Refinement*; Universität Göttingen: Göttingen, Germany, 1993.

(15) Supporting Information.

(16) (a) Childs, R. F.; Faggiani, R.; Lock, C. J. L.; Varadarajan, A. *Acta Crystallogr., Sect. C* **1984**, *40*, 1291–1294. (b) Suzuki, H.; Ishiguro, S. *Acta Crystallogr., Sect. E* **2006**, *62*, m576–578. (c) Hill, C. L.; Bouchard, D. A.; Kadkhodayan, M.; Williamson, M. M.; Schmidt, J. A.; Hilinski, E. F. *J. Am. Chem. Soc.* **1988**, *110*, 5471–5479.

(17) (a) Hunter, C. A.; Sanders, J. K. M. *J. Am. Chem. Soc.* **1990**, *112*, 5525–5534. (b) Hobza, P.; Selzle, H. L.; Schlag, E. W. *J. Phys. Chem.* **1996**, *100*, 18790–18794. (c) Sinnokrot, M. O.; Sherrill, C. D. *J. Phys. Chem. A* **2006**, *110*, 10656–10668. (d) Lee, E. C.; Kim, D.; Jurecka, P.; Tarakeshwar, P.; Hobza, P.; Kim, K. S. *J. Phys. Chem. A* **2007**, *111*, 3446–3457.

(18) (a) Matsuzakmi, S. Y.; Goto; Honda, K.; Kojima, I. *Anal. Sci.* **1995**, *11*, 461–463. (b) Camerman, A.; Trotter, J. *Acta Crystallogr.* **1965**, *18*, 636–643.

(19) (a) Fabbiani, F. P. A.; Allan, D. R.; Parsons, S.; Pulham, C. R. *Acta Crystallogr. B* **2006**, *62*, 826–842. (b) Desiraju, G. R.; Gavezzotti, A. *Acta Cryst., B* **1989**, *45*, 473–482. (c) Brock, C. P.; Dunitz, J. D. *Acta Crystallogr. B* **1990**, *46*, 795–806.

(20) Stasko, D.; Hoffmann, S. P.; Kim, K. C.; Fackler, N. L. P.; Larsen, A. S.; Drovetskaya, T.; Tham, F. S. *J. Am. Chem. Soc.* **2002**, *124*, 13869–13876.

(21) (a) Park, M.; Shin, I.; Singh, N. J.; Kim, K. S. *J. Phys. Chem. A* **2007**, *111*, 10692–10702. (b) Shin, I.; Park, M.; Min, S. K.; Lee, E. C.; Suh, S. B.; Kim, K. S. *J. Chem. Phys.* **2006**, *125*, 234305.

(22) (a) Lee, H. M.; Suh, S. B.; Lee, J. Y.; Tarakeshwar, P.; Kim, K. S. *J. Chem. Phys.* **2000**, *112*, 9759–9772. (b) Kim, J.; Kim, K. S. *J. Chem. Phys.* **1998**, *109*, 5886–5895.

(23) Suh, S. B.; Kim, J. C.; Choi, Y. C.; Kim, K. S. *J. Am. Chem. Soc.* **2004**, *126*, 2186–2193.

(24) Cho, H.-S.; Ha, N.-C.; Choi, G.; Kim, H.-J.; Lee, D.; Oh, K. S.; Kim, K. S.; Lee, W.; Choi, K. Y.; Oh, B.-H. *J. Biol. Chem.* **1999**, *274*, 32863–32868.

(25) (a) Lee, J. Y.; Hahn, O.; Lee, S. J.; Choi, H. S.; Shim, H.; Mhin, B. J.; Kim, K. S. *J. Phys. Chem.* **1995**, *99*, 1913–1918. (b) Kolaski, M.; Lee, H. M.; Choi, Y. C.; Kim, K. S.; Tarakeshwar, P.; Miller, D. J.; Lisy, J. M. *J. Chem. Phys.* **2007**, *126*, 074302.

JP101990F